PNAS RESEARCH ARTICLE | BIOCHEMISTRY CHEMISTRY

Proximity-activated DNA scanning encoded sequencing for massive access to membrane proteins nanoscale organization

Xueqi Zhao[a,b], Yue Zhao[b,1], Zhu Li[b], Huan Liu[b], Wenhao Fu[b], Feng Chen[b], Ying Sun[a,1], Daqian Song[a], Chunhai Fan[c,d], and Yongxi Zhao[b,e,1]

Affiliations are included on p. 9.

Edited by David Weitz, Harvard University, Cambridge, MA; received November 30, 2024; accepted February 17, 2025

Cellular structure maintenance and function regulation critically depend on the composition and spatial distribution of numerous membrane proteins. However, current methods face limitations in spatial coverage and data scalability, hindering the comprehensive analysis of protein interactions in complex cellular nanoenvironment. Herein, we introduce proximity-activated DNA scanning encoded sequencing (PADSE-seq), an innovative technique that utilizes flexible DNA probes with adjustable lengths. These dynamic probes are anchored at a single end, enabling free swings within a nanoscale range to perform global scanning, recording, and accumulating of information on diverse proximal proteins in random directions along unrestricted paths. PADSE-seq leverages the autonomous cyclic cleavage of single-stranded DNA to sequentially activate encoded probes distributed throughout the local area. This process triggers strand displacement amplification and bidirectional extension reactions, linking proteins barcodes with molecular barcodes in tandem and further generating millions to billions of amplicons embedded with the combinatorial identifiers for next-generation sequencing analysis. As a proof of concept, we validated PADSE-seq for mapping the distribution of over a dozen kinds of proteins, including HER1, EpCAM, and PDL1, in proximity to HER2 in breast cancer cell lines, demonstrating its ability to decode multiplexed protein proximities at the nanoscale. Notably, we observed that the spatial distribution of proximal proteins around low-abundance target proteins exhibited greater diversity across regions with variable proximity ranges. This method offers a massive access for high-resolution and comprehensive mapping of cellular molecular interactions, paving the way for deeper insights into complex biological processes and advancing the field of precision medicine.

membrane proteins | proximity detection | DNA encoding | nucleic acid amplification | high-throughput sequencing

Significance

Membrane proteins exhibit remarkable diversity and precise localization within dynamic nanoenvironments. Conventional methods are limited by modest protein variety and spatial coverage, hindering comprehensive profiling of membrane proteins. Thus, we developed proximity-activated DNA scanning encoded sequencing (PADSE-seq), which uses flexible and adjustable length of DNA scanning probes (SPs) and barcoding probes (BPs) to label target and proximity proteins. In PADSE-seq, hybridizations between SP and BP activate nicking endonucleases, resulting in the cleavage of BP and release of SP to cyclically search for nearby BP. The cleaved BP act as primers to initiate strand displacement amplification and bidirectional extension, generating tandem combinatorial barcodes for next-generation sequencing, which provides a massive access and global landscapes of membrane proteins nanoscale organization.

Membrane proteins, either embedded in or attached to cell membranes, are essential to biological processes such as material transport, signal transduction, and cell recognition, supporting both cellular function and structural integrity (1–3). These proteins move laterally within the phospholipid bilayer, guided by structures like lipid rafts and cytoskeleton, creating a highly organized distribution (4–7). Their dynamic mobility and spatial organization offer versatile regulatory mechanisms, enabling cells to adapt and function efficiently in ever-changing environments (8, 9). Profiling the spatial localization and proximity distribution of these proteins within the cell membrane provides valuable insights into their functions and interactions, shedding light on cellular dynamics at a molecular level and offering a deeper understanding of disease mechanisms (10–14).

With the rapid development and ongoing advancements in nucleic acids analysis, DNA has emerged as a prime candidate, offering distinct advantages for detecting and regulating proximal proteins at the nanoscale (15–21). For instance, DNA probes bound to two adjacent targets can undergo strand displacement, generating a fluorescence resonance energy transfer (FRET) signal (22, 23). This signal can be further amplified through isothermal amplification triggered by proximity-activated DNA hybridization, yielding enhanced fluorescence beyond what FRET alone can achieve (24). To improve spatial resolution, proximity-dependent point accumulation in nanoscale topography (PD-PAINT) and proximity PAINT (pPAINT), derived from the superresolution microscopy technique DNA-PAINT, have been introduced. When two proteins are in close proximity, split docking-site DNA probes on each protein hybridize to create a new binding site for fluorescent probes, enabling nanoscale visualization of protein proximities in pairs (25, 26).

Author contributions: X.Z., Yue Zhao, F.C., Y.S., and Yongxi Zhao designed research; X.Z., Yue Zhao, Z.L., and W.F. performed research; X.Z., Yue Zhao, H.L., W.F., D.S., C.F., and Yongxi Zhao analyzed data; and X.Z., Yue Zhao, and Yongxi Zhao wrote the paper.

The authors declare no competing interest.

This article is a PNAS Direct Submission.

[1]To whom correspondence may be addressed. Email: yuezhao@mail.xjtu.edu.cn, yingsun@jlu.edu.cn, or yxzhao@mail.xjtu.edu.cn.

This article contains supporting information online at https://www.pnas.org/lookup/suppl/doi:10.1073/pnas.2425000122/-/DCSupplemental.

Published April 10, 2025.

The above methods offer high-resolution observation of membrane protein interactions, yet are constrained by spectral overlap, which limits the variety of fluorescent labels available and in turn reduces the kinds of proteins that can be simultaneously detected. To overcome this limitation, a range of high-throughput approaches have been developed that combine DNA-conjugated antibodies with proximity extension or ligation assays, followed by PCR and next-generation sequencing (NGS) to enable broader profiling of diverse protein proximities (27–29). Furthermore, DNA hybridization or ligation, driven by target proximity, can regulate cell behaviors such as intracellular signal transduction, clustering of cell membrane receptors, cell protection, and motility (30–34). However, these aforementioned approaches depend on consumptive molecular reactions to record spatial positions, making it challenging to capture proximity information for more than two proteins at once, thus limiting the ability to provide a deeper insight into protein networks and cellular functions.

To decipher more complex molecular interactions within the nanoenvironments of membrane proteins, it is crucial to develop a method capable of simultaneously identifying and labeling the proximity distribution of multiple targets. Proximity labeling techniques use engineered enzymes to generate short-lived reactive molecules nearby, allowing rapid labeling of proximity molecules and enabling direct capture of transient or low-affinity protein interactions (35–38). However, their limited spatial resolution and insufficient reaction stability pose challenges for applications in complex biological systems. In response, DNA nanotechnology–based approaches have been introduced, providing high programmability and precise spatial control. Rolling circle amplification (RCA) generates barcodes with hundreds of repeated unique DNA sequences to cover and label molecules within defined regions. However, the challenge of precisely controlling size of RCA products compromises localization accuracy in proximity analysis, thereby limiting its utility in high-resolution studies of molecular interactions (39–41). Currently, a method termed nanoscale deciphering of membrane protein nanodomains (NanoDeep) has been proposed, which accurately translates protein organization information into DNA sequencing readouts via multiarm assembled DNA nanocomb probes (42). A molecular crawler system driven by polymerase and strand displacement can autonomously explore molecular spatial distributions by copying information from nearby encoded targets (43). The recently reported TETRIS (templated DNA repeats for analysis of interacting proteins) technology utilizes DNA-antibody-conjugated probes, combining bidirectional hybridization and covalent linking to linearize the barcodes of proximity proteins, enabling detailed analysis of interactions within higher-order protein complexes (44). These systems enable repeated, nondestructive sampling, allowing for high-resolution mapping of multivalent molecular interactions and complex molecular landscapes within cells.

However, proximity recognition in these methods relies on static or predesigned DNA nanoframeworks, which are constrained by inherent rigidity and fail to achieve comprehensive coverage of the nanoenvironment. Therefore, a method capable of flexibly spanning various directions to capture proximity information across diverse sites and regions remains to be developed. In our previous work, we reported cellular macromolecules-tethered DNA walking indexing (Cell-TALKING), where a DNA walking probe is tethered to target site and sequentially moves to activate nearby probes within the nanoenvironment, allowing for subsequent amplification and visualization via fluorescence imaging (41). Nevertheless, the intrinsic principles and modes of signal acquisition in fluorescence imaging still limit its ability to meet the demands of massive parallel molecular analysis. Herein, we introduce proximity-activated DNA scanning encoded sequencing (PADSE-seq) to expand the ranges of detectable proximity molecules. This approach employs a nucleic acid encoding strategy, embedding protein barcodes into proximity probes and molecular barcodes into amplification templates. With strand displacement amplification (SDA) to trigger bidirectional extension, it sequentially assembles the information of protein type identifiers (protein IDs) and molecular identifiers (molecular IDs) into DNA barcode combinations. Coupled with high-throughput sequencing, PADSE-seq facilitates the simultaneous profiling of various proximity proteins, providing a comprehensive landscape of their spatial organization at nanoscale.

Results

As shown in Fig. 1*A*, the DNA scanning probe (SP) tethered to the target site (T_0) starts in a blocked state and can be initiated by the nicking endonuclease (Nt.BbvCI, Nt). Once activated, it will sequentially trigger the activation of DNA barcoding probes (BPs) bound to adjacent sites (P_1, P_2, P_3, …, P_n) within the accessible region. Since the nicking reaction cleaves only one strand of DNA, the SP probe can be reset after undergoing a series of hybridization-nicking-release reactions and reinitiate subsequent cycles, ultimately activating all BP probes. By labeling with active groups, the above functional DNA probes can be conjugated to specific primary antibodies through a chemical coupling reaction to prepare antibody–DNA affinity probes (Ada probes) capable of binding cellular membrane proteins (Fig. 1*B*). The gray ellipses in Fig. 1*C* represent target proteins, which are recognized by specific antibodies labeled with SP probes. Proximity proteins are depicted as red, blue, and green ellipses, each capable of binding BP probes carrying unique sequences that represent protein IDs. The activated BPs feature a completely complementary 3′ end with template probes (TPs) and serve as a starting site for DNA polymerase (Klenow Fragment, 3′→5′ exo-, KF). These probes hybridize with TPs containing distinct molecular IDs, triggering polymerase extension and creating nicking recognition sites. This process initiates SDA, releasing encoded products that combine both protein IDs and molecular IDs in tandem. The amplicons are then subjected to PCR and NGS for profiling the spatial distribution of various membrane proteins.

We first validated the feasibility of using nicking endonuclease to continuously activate BP probes in solution reactions. To achieve this, we designed a set of probes with distinct functions, some labeled with specific fluorescent groups (SPsol, BPsol-Cy3, and TPsol-Cy5), the detailed sequences information of which are provided in *SI Appendix*, Table S1. As shown in Fig. 2*A*, the BPsol-Cy3 probe is composed of multiple functional domains, including the PCR primer–binding region (purple), polymerase extension region (green), nicking endonuclease recognition region (blue), and the blocked region (gray) labeled with a Cy3 fluorophore. The SPsol is partially complementary to BPsol-Cy3, forming a duplex hybrid complex with overhanging 3′ ends on both strands. The central hybridization region creates a recognition site for nicking endonuclease. Upon nicking action, the previously stable duplex is disrupted due to a single-strand break, causing strand dissociation. The released SPsol can cyclically activate BPsol-Cy3 dispersed in solution under the action of nicking endonuclease. TPsol-Cy5 consists of a polymerase extension region (gray segment at the 5′ end), a nicking endonuclease recognition region (blue), a spacer domain (red), a BP-binding domain, and a blocked region at 3′ end modified with a Cy5 fluorophore. Activated BPsol-Cy3 completely complements with TPsol-Cy5 and possesses a 3′ hydroxyl group recognizable by polymerase, regenerating a duplex structure with a nicking endonuclease recognition site after extension, thereby initiating the SDA reaction. In contrast, if the BPsol-Cy3

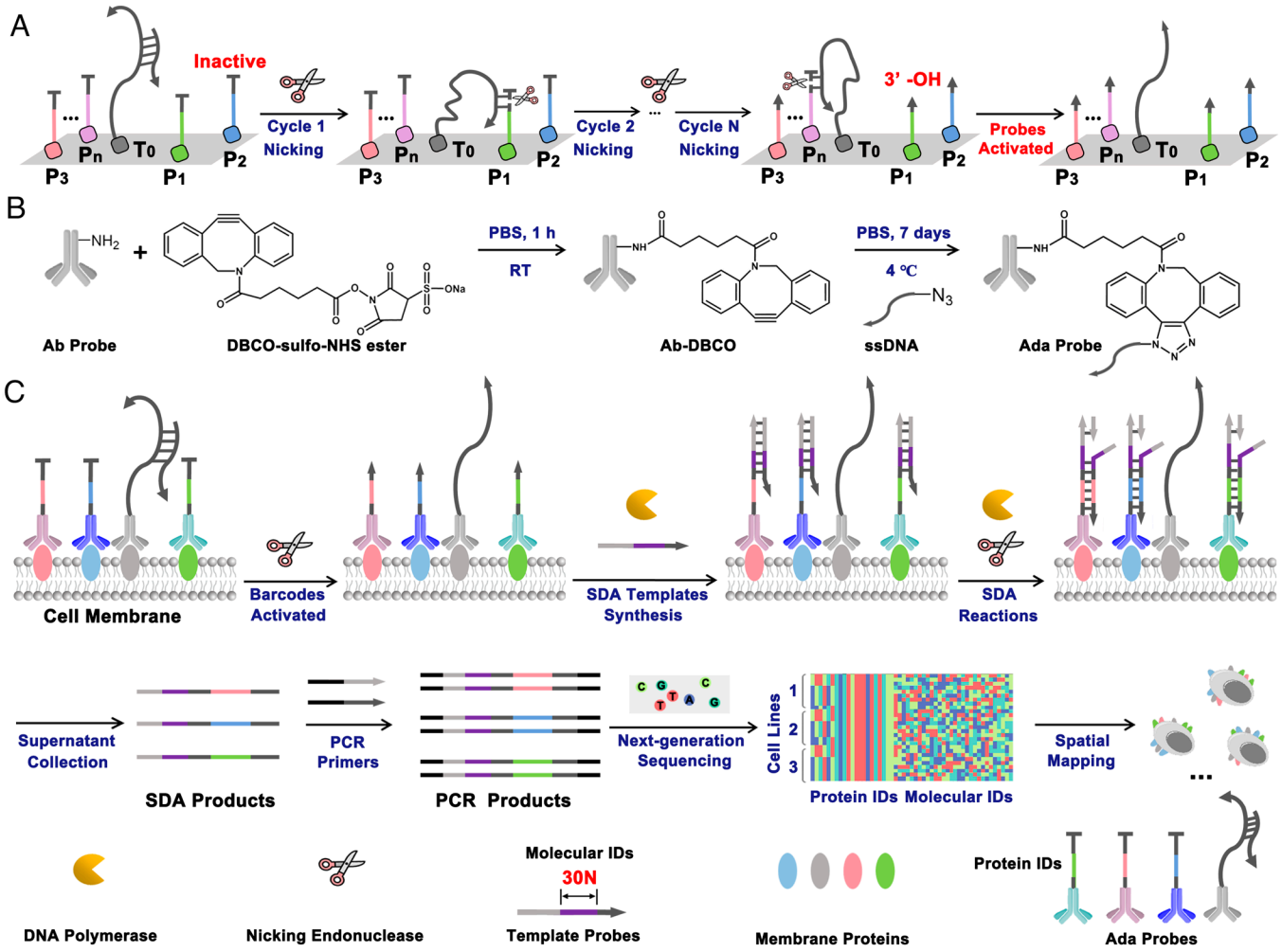

Fig. 1. Schematic illustration of PADSE-seq. (*A*) A conceptual diagram depicting the sequential activation of proximity probes located at nearby sites (P_1, P_2, P_3, ..., P_n) by the scanning probe at the target site (T_0). (*B*) The principles and reaction processes for the synthesis of Ada probe. (*C*) A schematic workflow of PADSE-seq for recording and mapping the nanoscale organization of cellular membrane proteins. Ab probe represents primary antibody. DBCO-sulfo-NHS ester represents Dibenzocyclooctyne-sulfo-N-hydroxysuccinimidyl ester. Ab-DBCO represents DBCO-sulfo-NHS ester modified Ab probe. ssDNA represents single-stranded DNA. Ada probe represents antibody–DNA affinity probe. RT represents room temperature.

is not activated by SPsol, it would still partially hybridize with TPsol-Cy5. However, the resulting hybrid product will have mismatched and overhanging 3′ ends on both strands, preventing effective polymerase extension and subsequent reactions. To demonstrate the cyclic activation function of the SPsol probe, we set the concentration ratio of SPsol to BPsol-Cy3 at 1:5. Stepwise reaction products were analyzed using polyacrylamide gel electrophoresis (PAGE). As shown in Fig. 2*B*, SPsol was complementary to BPsol-Cy3, forming a double-stranded hybrid structure. A small amount of SPsol cyclically activated the excess BPsol-Cy3, leading to the generation of Cy3-labeled short DNA fragments and the cleavage of BPsol-Cy3, which subsequently initiated the SDA reaction. In contrast, in the absence of Nt or SPsol, BPsol-Cy3 remained inactive, and neither amplification nor SDA occurred.

We then utilized sequence length as barcodes to distinguish different types of BP probes, verifying the capability of PADSE-seq to activate multiple encoded probes. Four BPsol probes with varying lengths of polymerase extension regions (BPsol-0, BPsol-10, BPsol-20, and BPsol-30) were designed, all sharing identical PCR primer–binding regions. Following SDA, these probes underwent PCR amplification and electrophoresis characterization under consistent conditions. As illustrated in Fig. 2*C* and *SI Appendix*, Fig. S1, both electrophoresis and melting curve analyses confirmed the generation of four distinct amplification products corresponding to the four BPsol probes. The lengths of products increased incrementally as predicted based on the length barcodes. Notably, no product bands were detected in the absence of SPsol, further supporting the specificity of our method. We additionally introduced sequence barcodes into the PCR primer–binding regions of BP probes. This design allowed specific recognition of different BPsol probes by three distinct PCR primers, resulting in amplification products labeled with Cy3, Cy5, or FAM fluorophores. Fig. 2*D* and *SI Appendix*, Fig. S2 presented the multicolor gel electrophoresis imaging analysis of PCR products generated by various combinations of BPsol probes (BPsol-1, BPsol-2, and BPsol-3). The three fluorescently labeled primers (FP-FAM, FP-Cy3, and FP-Cy5) specifically recognized the corresponding SDA products generated in the upstream reactions. In the first two samples, where neither SPsol nor BPsol was added, no significant intensity peak of product was observed. In contrast, the third to ninth samples exhibited distinct combination peaks corresponding to one, two, or three fluorescent products, respectively. These results further confirmed the effectiveness of PADSE-seq in recognizing and activating encoded probes and producing the corresponding amplification products.

To further demonstrate the proximity recognition and recording capabilities of PADSE-seq at nanoscale, we conducted interface

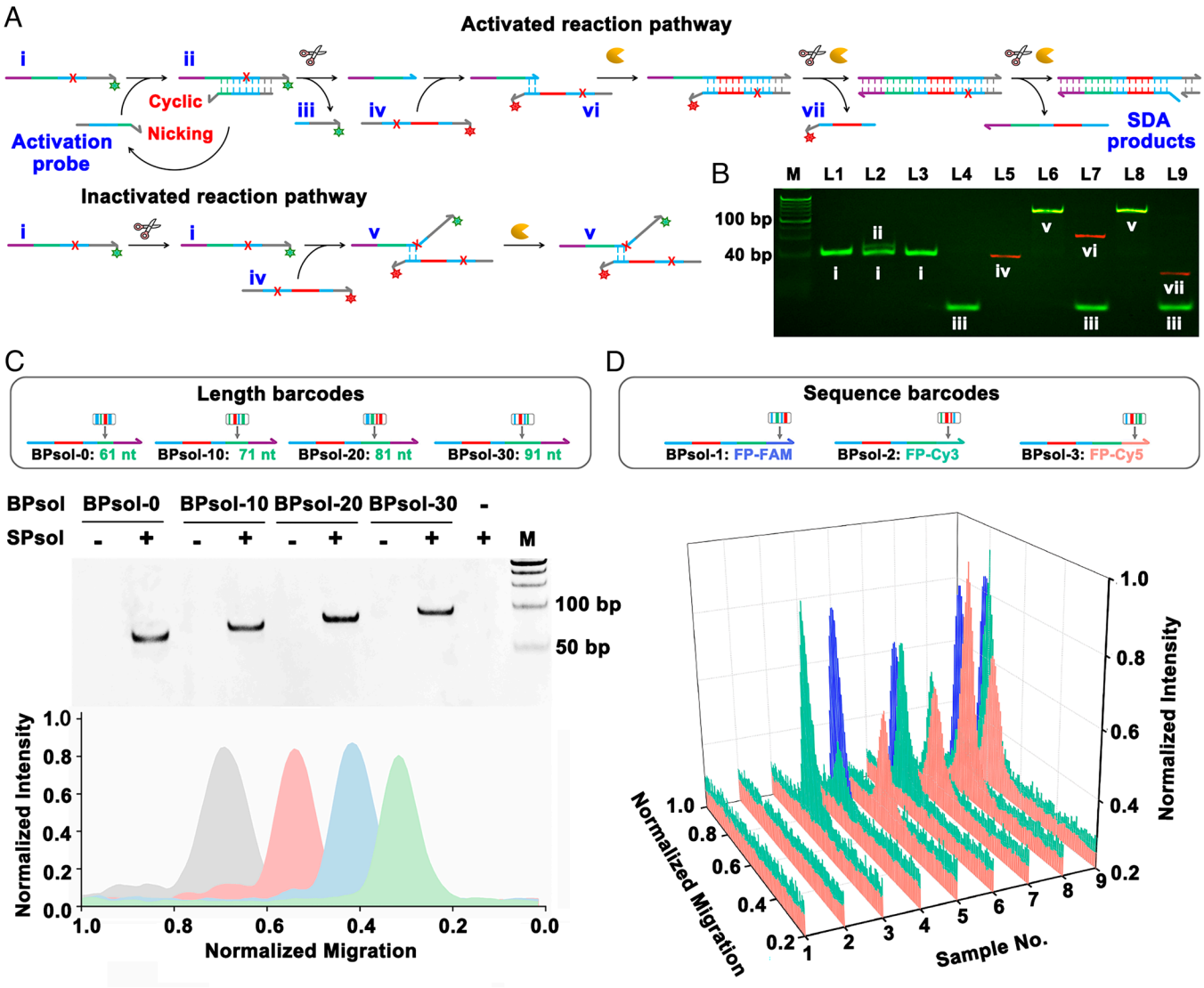

Fig. 2. In vitro validation of endonuclease-mediated continuous activation of BP probes. (*A*) Reaction mechanism of cyclic nicking and sequential activation of barcoding probes (BPsol-Cy3) by the scanning probe (SPsol). Reactants and products at each stage are denoted with Roman numerals. i) BPsol-Cy3; ii) duplex formed between SPsol and BPsol-Cy3; iii) cleaved BPsol-Cy3; iv) TPsol-Cy5; v) duplex formed between inactivated BPsol-Cy3 and TPsol-Cy5; vi) duplex formed between activated BPsol-Cy3 and TPsol-Cy5; vii) cleaved TPsol-Cy5. The green star at the end of BP probe represents the Cy3 fluorophore, while the red star indicates the Cy5 fluorophore. (*B*) Gel electrophoresis of the products at each stage. L1: BPsol-Cy3; L2: BPsol-Cy3 +SPsol; L3: BPsol-Cy3 +Nt; L4: BPsol-Cy3 +SPsol +Nt; L5: TPsol-Cy5; L6: BPsol-Cy3 +TPsol-Cy5 +Nt; L7: BPsol-Cy3 +SPsol +Nt +TPsol-Cy5; L8: BPsol-Cy3 +Nt +TPsol-Cy5 +KF; L9: BPsol-Cy3 +SPsol +Nt +TPsol-Cy5 +KF. M represented 20 bp DNA ladder. (*C*) Diagrammatic sketch of SDA products with different length barcodes (*Top*). Gel electrophoresis of PCR products and control groups of BPsols with length barcodes (BPsol-0, BPsol-10, BPsol-20, and BPsol-30) (*Middle*). PAGE analysis of PCR products in the *Middle* part, the peaks from *Left* to *Right* corresponding to BPsol-0, BPsol-10, BPsol-20, and BPsol-30, respectively (*Bottom*). M represented 50 bp DNA ladder. (*D*) Diagrammatic sketch of SDA products with different sequence bar-codes (*Top*). PAGE analysis with multicolor fluorescence channels gel imaging. The PCR products from reactions involving various BPsols with sequence barcodes (BPsol-1, BPsol-2, and BPsol-3) could be amplified using various primers labeled with specific fluorophores (FP-FAM, FP-Cy3, and FP-Cy5) (*Bottom*). No.1: negative control without SPsol; No.2: negative control without BPsols; No.3: BPsol-2; No.4: BPsol-1; No.5: BPsol-3; No.6: BPsol-1 +BPsol-2; No.7: BPsol-2 +BPsol-3; No.8: BPsol-1 +BPsol-3; No.9: BPsol-1 +BPsol-2 + BPsol-3. Nt represents the nicking endonuclease Nt.BbvCI; KF represents the DNA polymerase Klenow Fragment (3′→5′ exo-).

experiments leveraging the high programmability and precise spatial control of DNA origami to mimic the complex molecular proximity distributions on cell membrane surfaces. First, we designed and synthesized DNA origami structures with functional protruding ends (Fig. 3 *A*, *Left*), and confirmed their assembly using atomic force microscopy (AFM) imaging (Fig. 3 *A*, *Right*) (45). The protruding ends were arranged on three concentric circles with radii of approximately 10, 20, and 30 nm from the central target site. Detailed sequences and positional information of the target sites are provided in *SI Appendix*, Fig. S3 and Table S2 Protruding strands at different sites on the origami were predesigned to hybridize with SP or BP probes. This allowed the SP probe to be anchored at the central target site, while BP probes carrying positional information were distributed at specific positions along the three concentric circles. The SP probes could continuously activate adjacent BP probes in a cyclic cleavage reaction (Fig. 3*B*), triggering subsequent SDA and PCR reactions to generate PCR products with distinct positional information. To simplify identification, the BP, SP, and TP probes used in the DNA origami validation experiments were designated as BPori, SPori, and TPori, respectively. Certain functional regions were modified or adjusted as needed based on the solution-phase probes used (*SI Appendix*, Fig. S4). Notably, during the synthesis of DNA origami, SPori required initial blocking to prevent premature hybridization with BPori. To achieve this, a blocking strand (Assori) was introduced to

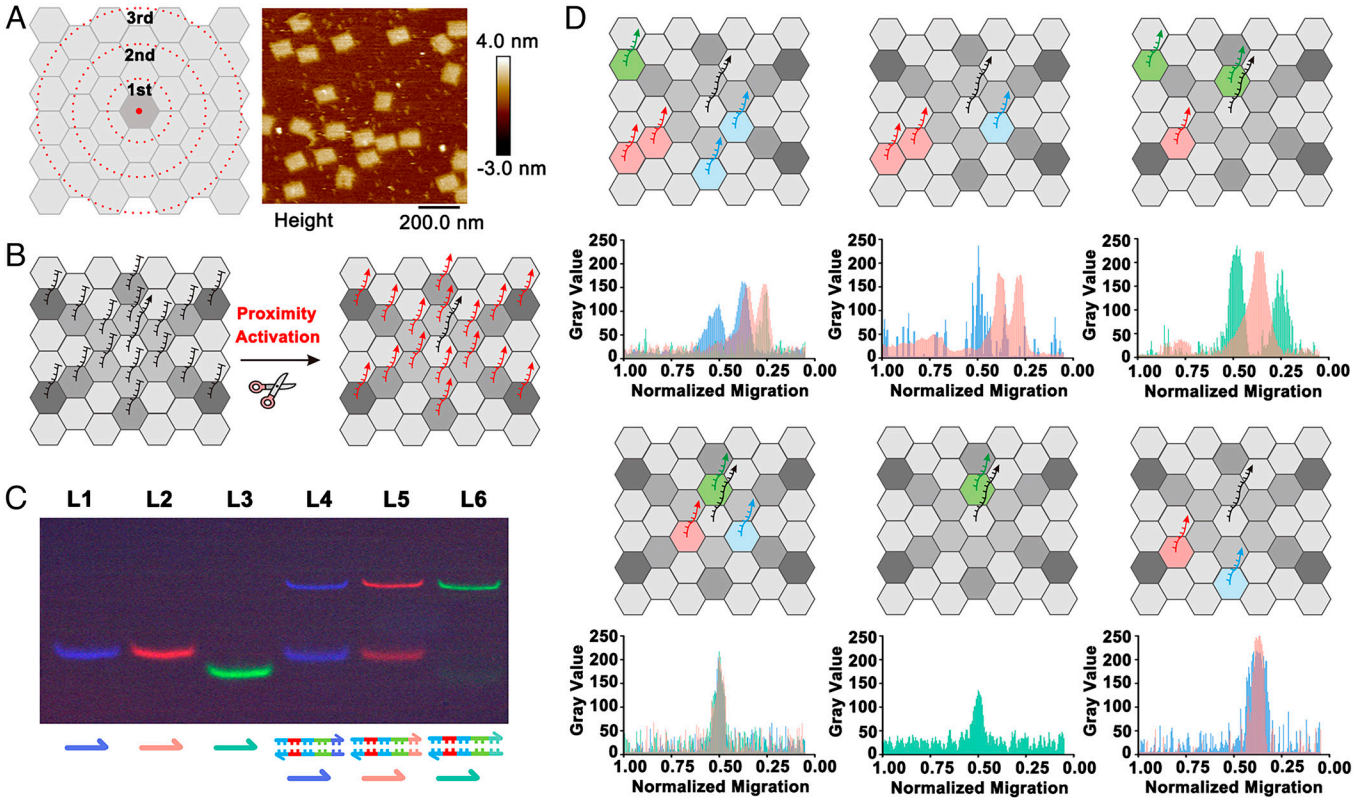

Fig. 3. Validation of PADSE-seq on DNA origami. (*A*) Structural design of DNA origami and corresponding AFM images. Protruding strands are positioned on three concentric circles with different radii to bind adjacent sites at varying distances. The first, second, and third circles are located approximately 10 nm, 20 nm, and 30 nm away from the central target site, respectively. (Scale bar, 200 nm.) (*B*) Schematic illustration of the activation of proximity barcode probes on DNA origami. Black arrows represent SPori probes bound to the central target sites, while red arrows indicate the activated proximity barcode probes (BPori). (*C*) Gel electrophoresis of PCR products generated from activated BPori probes on the three circles of the origami. Lanes L1 to L3 represented samples without SPori; while lanes L4 to L6 represented samples with SPori. To distinguish PCR products from different activated probes, BPori probes in different circles were paired with PCR primers carrying unique fluorescence labels (FP29t-FAM, FP110 s-Cy5, and FP48f-Cy3, 29t, 110s and 48f correspond to specific positions on the DNA origami in *SI Appendix*, Fig. S3). Specifically, L1 and L4 corresponded to FP29t-FAM, L2 and L5 corresponded to FP110s-Cy5, and L3 and L6 corresponded to FP48f-Cy3. (*D*) PAGE analysis of complex proximity distributions. To further distinguish PCR products from different activated probes, the lengths of BPori probes were designed to increase with the circle number, resulting in distinct migration during gel electrophoresis. And BPori probes within the same circle were distinguished with different fluorescent PCR primers. Forward primers (FP) labeled with FAM are shown in blue, those labeled with Cy3 are shown in green, and those labeled with Cy5 are shown in red. Detailed site information is provided in *SI Appendix*, Fig. S6.

form a stable duplex with SPori. This duplex was designed to be cleaved by nicking endonuclease, efficiently releasing SPori and enabling it to activate adjacent BPori probes. To meet these requirements, we incorporated continuous nicking endonuclease recognition sequences into the complementary region of Assori and SPori. Once Assori was cleaved into fragments, it could no longer form a stable hybrid structure, thereby releasing SPori to complete subsequent reactions.

We first validated the ability of SPori probes, anchored at the central site of the DNA origami, to recognize and activate adjacent BPori probes distributed on three concentric circles. The BPori probes on these circles were designed with distinct PCR primer–binding regions serving as positional barcodes. These sequences were specifically recognized and amplified by PCR primers labeled with different fluorophores, generating fluorescently tagged PCR products (Fig. 3*C* and *SI Appendix*, Fig. S5). To further demonstrate capability of PADSE-seq to analyze complex distributions of proximity sites, we designed six DNA origami structures with varying BPori distributions (Fig. 3*D* and *SI Appendix*, Fig. S6). To distinguish the PCR products corresponding to different BPori probes during electrophoresis, we combined fluorescent groups labeling with length variation of products. Specifically, PCR products of BPori probes from the same circle were labeled with primers carrying different fluorophores, generating products with distinct fluorescence signals. Additionally, the lengths of PCR products from sites on each circle progressively increased outward from the first circle. The results showed the relationship between the grayscale values of fluorescent bands in electrophoresis imaging and their normalized migration distances. As the lengths of products increased, migration rates decreased, while PCR product peaks corresponding to probes on the same circle closely overlapped. Meanwhile, we analyzed the PCR products using real-time quantitative PCR (qPCR) and Sanger sequencing, with partial data shown in *SI Appendix*, Figs. S7 and S8. These results confirmed that the SPori probes could effectively activate BPori probes and PADSE-seq successfully captured the nanoscale spatial distribution of proximity sites.

We designed two types of DNA origami substrates with different distributions of proximity probes to simulate the changes in the spatial proximity of membrane proteins within complex cellular nanoenvironments. As shown in Fig. 4*A* and *SI Appendix*, Fig. S9, we introduced template probes (TPcel) containing 30 N (random sequences of A, T, C, or G) to encode each activated BPori probe. These random sequences served as molecular IDs for analyzing the proportions of various proximity molecules in sequencing results. Additionally, barcode sequences were incorporated into BPori probes to represent protein IDs. During subsequent SDA reactions, molecular IDs and protein IDs were concatenated and amplified via PCR, resulting in products with distinct characteristic regions and fixed lengths (*SI Appendix*, Fig. S10). These products were then subjected

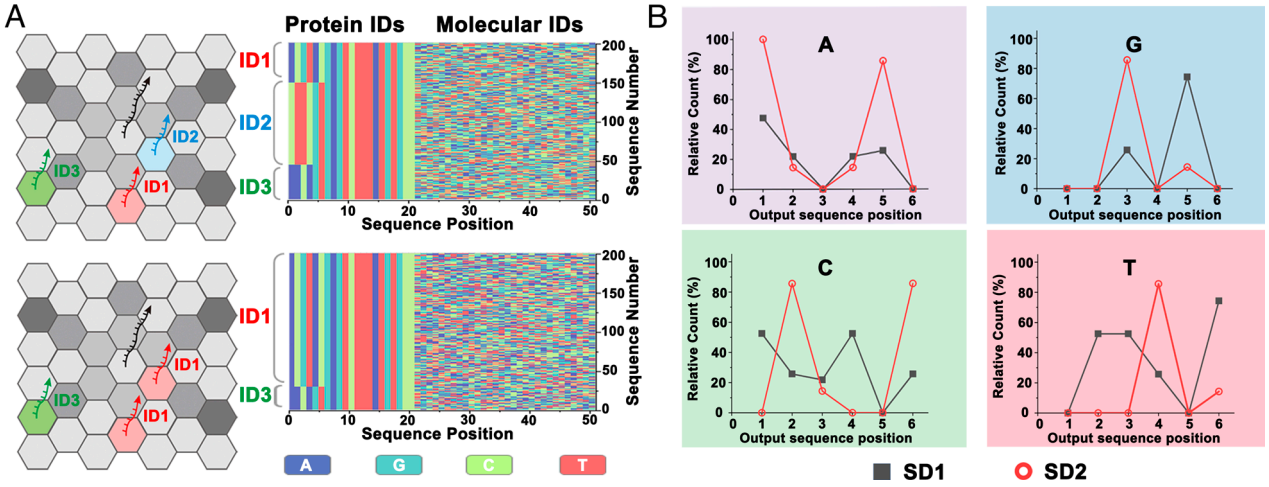

Fig. 4. PADSE-seq analysis of the molecular proximity distributions on DNA origami interfaces. (*A*) Schematic illustration of the distribution patterns of various proximity molecules (*Left*). NGS results of products derived from DNA origami substrate 1 (SD1) and substrate 2 (SD2) (*Right*). The *x*-axis represented the 51-mer bases composition of sequencing readouts, the *y*-axis (arbitrary) indicated the sequence number within the analyzed set. (*B*) Relative frequency of A, G, C, and T across the first six positions (representing distinct protein IDs) from the NGS data shown in Fig. 4*A*.

to NGS for further data interpretation. The SPori probes on both DNA origami substrates were positioned at the central site and remained unchanged. On substrate 1 (SD1), BPori probes carrying three distinct protein IDs (BP1-1, BP1-2, and BP1-3) were placed on three concentric circles at different radial distances from the center. Meanwhile, on substrate 2 (SD2), the BP2-1 probe with the same protein ID as BP1-2 was introduced on the innermost circle, mimicking changes in membrane protein distribution on the cell surface. Excluding the forward and reverse primers, the target product sequences were 51 bp in length. After filtering and error correcting, sequences of the desired length were obtained, and the first six bases were matched with predefined protein ID sequences for a second round of selection. Based on the sequencing results, we statistically analyzed the barcode proportions and randomly selected 200 reads for visualization with equal probability (Fig. 4 *A*, *Right*). In the results from SD1, a substantial number of barcodes representing three types of BPori probes were observed, corresponding to the protein IDs for membrane protein analysis. In contrast, the results from SD2 revealed that the involvement of a newly encoded probe at the designated site resulted in the absence of protein ID2 information, which had been associated with the first-circle probe on the SD1. Instead, a notable increase in sequencing reads corresponding to protein ID1 was observed. The proportion of the barcode "ACGTAC" in SD2 was approximately equal to the combined proportions of "ACGTAC" and "CTTCGT" in SD1. Further analysis of the base counts at the first six positions, which represented protein kinds across the entire read set (Fig. 4*B*), revealed consistent trends reflecting these proportional changes. These results demonstrated a strong correlation between the sequencing outcomes and the spatial distribution of proximity sites, highlighting the potential of this approach for profiling actual membrane protein proximity distributions.

To validate the feasibility of PADSE-seq for analyzing the proximity distribution of membrane proteins in cells, we selected over a dozen kinds of membrane proteins from breast cancer cell lines. Among these, EpCAM and PDL1 are common tumor markers, while HER2 overexpression is a hallmark of breast tumors. Additionally, the heterodimerization of epidermal growth factor receptor (HER1) and HER2 has been widely reported in previous studies (46, 47). Using Dibenzocyclooctyne-sulfo-N-hydroxysuccinimidyl ester (DBCO-sulfo-NHS ester) as a linker, primary antibodies targeting these four proteins were conjugated to single-stranded DNA (ssDNA) carrying azide groups to generate Ada probes, enabling specific recognition of their respective target proteins (48). These ssDNA were listed in Probes for PADSE-seq on fixed cells of *SI Appendix*, Table S1. Then, the preparation of Ada probes was characterized by PAGE analysis. As shown in *SI Appendix*, Fig. S11, the migration of the DNA-antibody-conjugates was significantly shifted compared to the DNA probes alone, indicating successful functionalization of the primary antibodies with DNA. The prepared Ada probes and primary antibodies (Ab probes) were used to label MDA-MB-468 breast cancer cells, followed by staining with Alexa Fluor 488-conjugated secondary antibodies. As shown in Fig. 5*A*, both probes displayed nearly identical fluorescence intensities. To further validate this observation, fluorescence intensity analysis was performed on twenty randomly selected cells per group under the Alexa Fluor 488 channel. The results revealed similar fluorescence intensity distributions between the Ada probes and Ab probes, indicating that the prepared Ada probes retained the ability of primary antibodies to specifically recognize and bind their target proteins (Fig. 5*B*).

The molecular reaction mechanism on the cell surface is illustrated in Fig. 6*A*. The process initiates with specific recognition of various proteins by their corresponding Ada probes. Following this recognition event, the SP probe, activated by a nicking endonuclease, undergoes cyclic cleavage, sequentially triggering the activation of BP probes. To ensure activation efficiency, we reverified the release and cyclic activation performance of the SP probe designed for cells (*SI Appendix*, Fig. S12). Upon activation, BP undergoes 3′ end processing where mismatched sequences are removed, enabling the hybridization with TP to form a complementary primer region suitable for DNA polymerase-mediated extension. During polymerization, BP serves as a primer to extend along TP, integrating the specific protein IDs with the molecular IDs present on TP and enabling combinatorial encoding. Additionally, the 5′ end of TP is designed to form a specific recognition sequence for nicking endonuclease cleavage upon extension. This allows the extended product to be recleaved, generating a new priming site on TP and triggering reverse extension. This process initiates SDA to achieve a signal amplification and efficiently releases amplified barcode products. The products with tandem barcodes are then analyzed using PCR and NGS, providing a comprehensive mapping of the proximity distribution of multiple cell surface proteins.

As a proof of concept, we first selected four different membrane proteins, specifically the SPcel probes were functionalized on primary antibodies against HER2 (referred to as HER2-Ada), while BPcel probes with distinct protein barcodes were conjugated to primary antibodies for the other three proteins, named HER1-Ada,

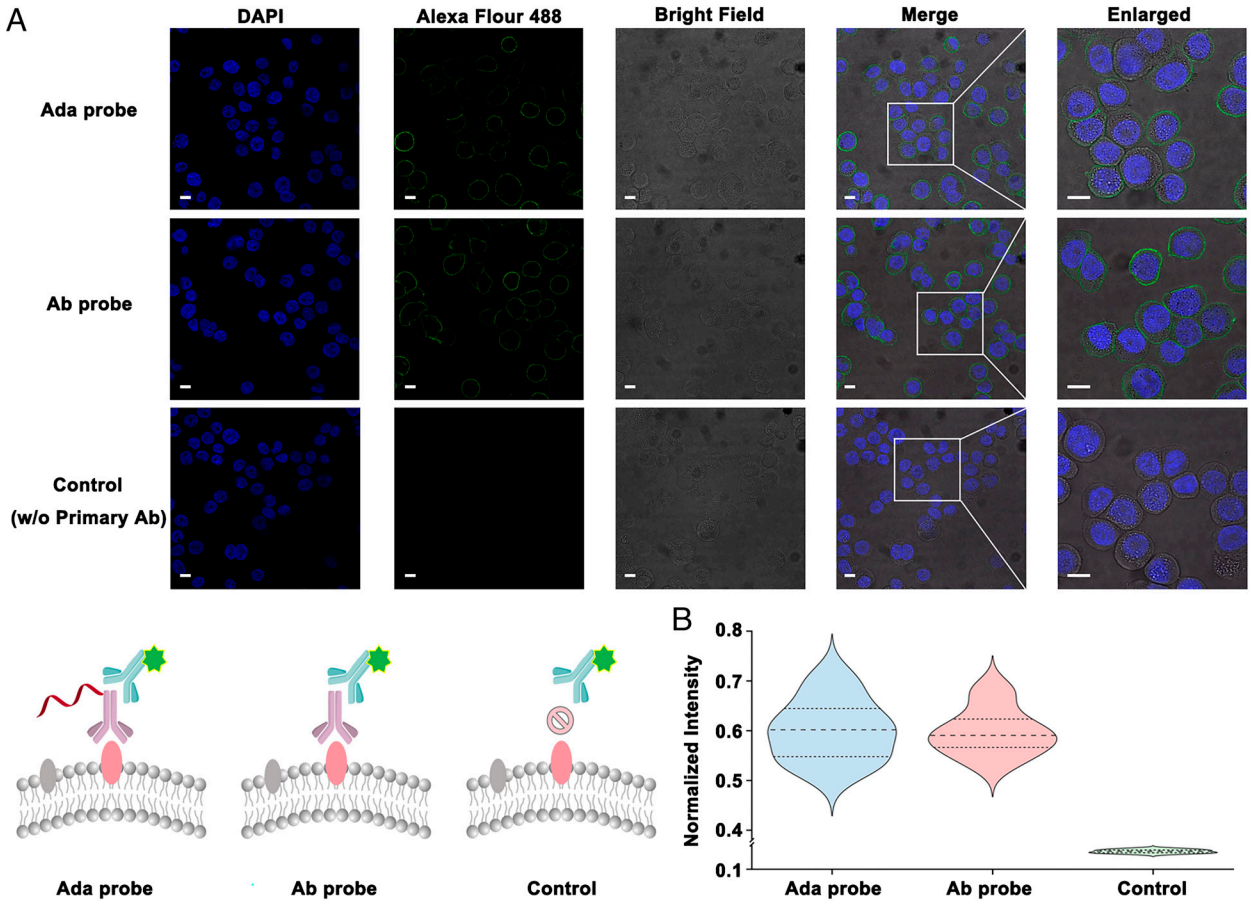

Fig. 5. Performance evaluation of Ada Probes. (*A*) Fluorescence imaging of MDA-MB-468 breast cancer cells. Cells were labeled with HER1-specific Ada and Ab probes, followed by staining with Alexa Fluor 488-conjugated secondary antibodies. The nuclei were stained with DAPI. All scale bars were 10 μm. (*B*) Statistical analysis of Alexa Fluor 488 fluorescence intensity from imaging results of MDA-MB-468 cells labeled with Ada probes, Ab probes, and negative control. A total of twenty cells were analyzed for each statistical analysis.

EpCAM-Ada, and PDL1-Ada, respectively. The proximity range was adjustable by varying the lengths of the SPcel and BPcel probes (Fig. 6*B*). Given that each base pair corresponds to approximately 0.34 nm, a 30-base-pair sequence corresponds to a length of about 10 nm. Accordingly, the proximity distances of the two sets of SPcel and BPcel probes were estimated to be about 30 nm and 40 nm, respectively. The estimation was solely intended for comparative analysis within a relative range, primarily calculated based on simplified model parameters including base counts and persistence length, while temporarily excluding the influence of other environmental factors (49, 50). Given the complexity of cellular components, we initially assessed the distribution of HER2 in proximity to HER1 in SK-BR-3 cells, optimized the reaction conditions, and verified the accuracy of the product sequences via Sanger sequencing. To evaluate the specificity of PADSE-seq in cellular analysis, we conducted a series of negative control experiments, including groups lacking HER2-Ada, HER1-Ada, or all primary antibodies. As shown in *SI Appendix*, Fig. S13, the qPCR fluorescence curves validated the successful generation of the expected PCR products in both parallel experimental groups, while no signals were detected in the negative controls. Gel electrophoresis further supported these findings, displaying a single band of the anticipated length in the experimental lanes, with no bands visible in the control lanes (*SI Appendix*, Fig. S14). Moreover, the Sanger sequencing results were fully consistent with the expected sequences (*SI Appendix*, Fig. S15). We then applied PADSE-seq to map the protein composition within the nanoscale proximity regions of HER2 in SK-BR-3, BT-474, and MCF-7 cells. Negative controls included variables without HER2-Ada, without HER1-Ada, EpCAM-Ada, and PDL1-Ada or without all primary antibodies. The PCR products from these groups were first characterized by PAGE (products in one of the groups are shown in *SI Appendix*, Fig. S16). Subsequently, the PCR amplification products from the experimental groups were analyzed using NGS. Following a process similar to the analysis of DNA origami interfaces, sequences were filtered, and the barcodes corresponding to the three proteins were tallied. The arbitrary subsets of sequencing readouts with color-coded bases are shown in *SI Appendix*, Figs. S17 and S18. As depicted in Fig. 6*C* and *SI Appendix*, Fig. S19, the counts were normalized, and the proportions of HER1, EpCAM, and PDL1 at varying proximity distances were calculated for each cell line. The statistical results revealed that the distribution of the three proteins around HER2 was consistent across all cell lines, with EpCAM showing the highest proportion in the HER2 proximity region and PDL1 the least. While the trends in protein proportions were similar under all conditions, slight variations were observed in the exact values. Notably, changes in protein proportions were more pronounced in MCF-7 cells compared to the other two cell lines as the proximity distance increased. This may be attributed to the relatively low expression level of HER2 in MCF-7 cells, which reduced the overlapping area covered by different probes, resulting in more significant changes when the scanning area was expanded. To further demonstrate the multiplexing capability of PADSE-seq across a broader range of proximity proteins, we designed additional Ada probes targeting other ten kinds of proteins (characterization shown in *SI Appendix*, Fig. S20) and applied them to SK-BR-3 cells (Fig. 6*D*). This enabled us to simultaneously profile 13 proximity

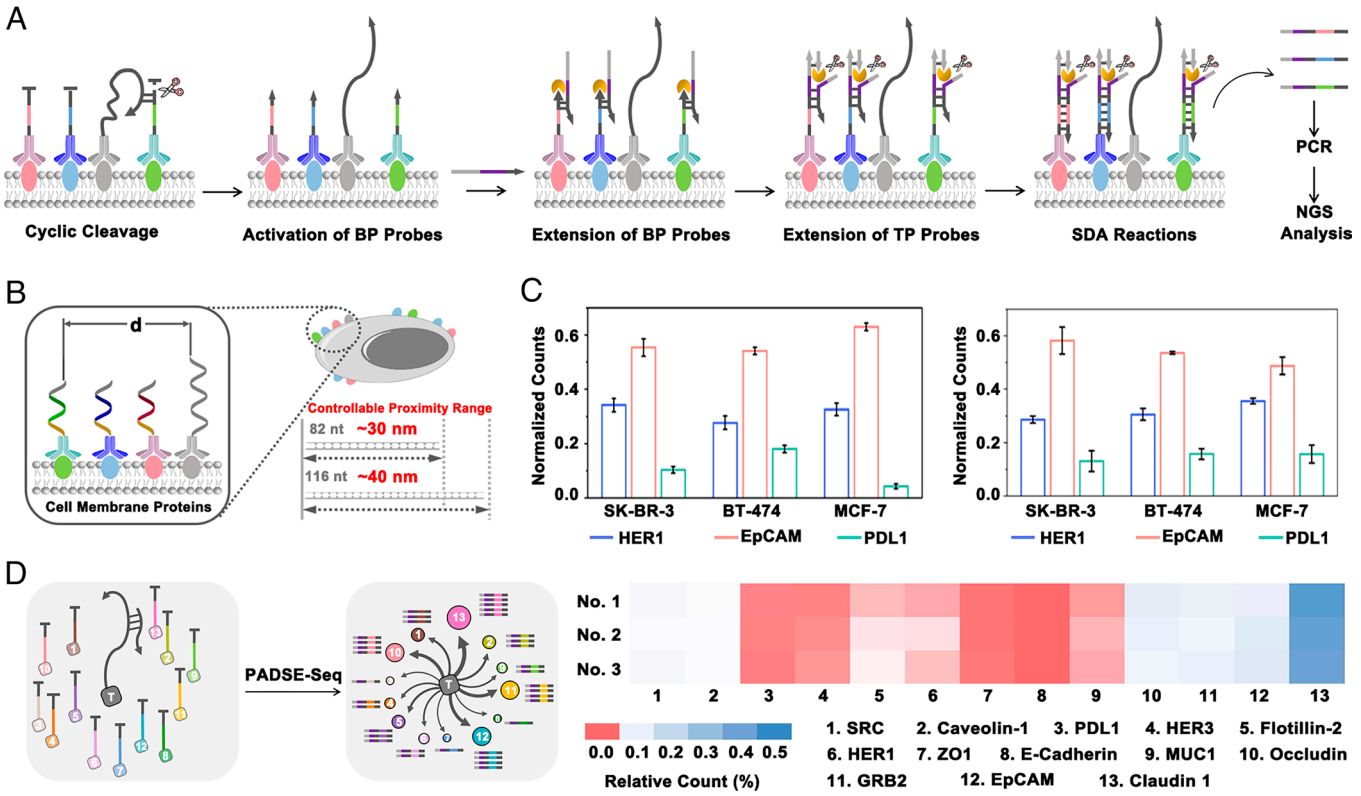

Fig. 6. PADSE-seq analysis of the nanoscale organization of membrane proteins in breast cancer cell lines. (*A*) Schematic illustration of molecular reaction mechanism on the cell surface. The scissors icon denoted the nicking endonuclease, whereas the notched circle icon represented the polymerase. (*B*) Schematic representation of the controllable nanoscale proximity range by varying the length of Ada probes. (*C*) Distribution proportions of HER1, EpCAM, and PDL1 within approximately 30 nm (*Left*) and 40 nm (*Right*) proximity regions around Her2 in SK-BR-3, BT-474, and MCF-7 cells. Data were presented as mean ± SD, with error bars indicating SD (n = 3). (*D*) PADSE-seq analysis of multiple membrane proteins. A conceptual view of PADSE-seq for profiling a dozen kinds of proteins. The gray squares depict target protein bound by SP, while colored circles indicate proximity proteins captured by BP, with circle sizes proportional to the relative abundance of corresponding proteins (*Left*). Heatmap display of the relative distribution of 13 kinds of proximity proteins around HER2 in SK-BR-3 cells. The three sequential numbers represent three independent parallel experiments (*Right*).

proteins surrounding HER2. As shown in Fig. 6*D* and *SI Appendix*, Fig. S21, among the 13 proximity proteins analysis, Claudin 1 exhibited the highest distribution ratio. In summary, we have established a method capable of mapping the proximity distributions of membrane proteins at nanoscale in fixed cells.

Discussion

In this work, we present an innovative approach to decipher the nanoscale spatial proximity distribution of membrane proteins. The PADSE-seq method we developed skillfully integrates cyclic enzymatic reactions with template amplification, enabling the resetting of scanning probes and sequential activation of multiple proximity barcode probes. This method enables the tandem assembly of protein barcodes with molecular identifiers, allowing simultaneous recording of protein types and quantities at multiple proximity sites. The resulting extensive information is then converted into numerous DNA products and decoded through high-throughput sequencing.

This breakthrough addresses the limitations of traditional proximity hybridization or ligation-based methods, which rely on consumable probes and are confined to one-to-one proximity information, establishing a one-to-many mapping strategy for multivalent interactions. Moreover, the scanning probes, with their flexibility and adjustable length, enable free and random movement in both direction and path, which overcomes the coverage deficiencies associated with DNA nanostructure probes or fixed motion modes during multisite recognition, thereby ensuring comprehensive exploration of the proximity region.

The method can also be adapted to accommodate a wider variety of target molecules, such as chemical conjugation to nucleic acid epigenetic modification sites, nucleic acid aptamers, or nanobodies. Smaller recognition modules offer the potential for even higher spatial resolution (15, 51–55). With over a dozen kinds of membrane proteins as a proof of concept, we demonstrated the feasibility of PADSE-seq in mapping the spatial proximity distribution of membrane proteins. By introducing DNA barcode sequences, this method theoretically enables the simultaneous analysis of proximity distributions for dozens or even hundreds of different proteins.

In conclusion, we present PADSE-seq as a versatile and promising platform with robust large-scale data processing capabilities, designed for the precise analysis of the nanoscale organization of membrane proteins. Looking ahead, PADSE-seq has the potential to be applied to a wide range of complex molecular interactions, including signal transduction pathways, nucleic acid–protein interactions, and virus–host dynamics. This method holds significant promise for uncovering spatial molecular relationships and intricate interaction networks across diverse biological systems.

Materials and Methods

The complete description of the materials and methods is provided in *SI Appendix, Materials and Methods*. The NGS data generated in this study have been deposited in the National Center for Biotechnology Information (NCBI) Sequence Read Archive (SRA) database under accession code PRJNA1185922 and PRJNA1221128 (56, 57).

Data, Materials, and Software Availability. NGS sequencing data have been deposited in NCBI SRA (PRJNA1185922 and PRJNA1221128) (56, 57).

ACKNOWLEDGMENTS. We acknowledge the support of the National Natural Science Foundation of China (Nos. 22125404, 22004096, and 22474107), the National Key Research and Development Program of China (No. 2023YFB3210103), the Natural Science Foundation of Shaanxi Province (No. 2023JC-JQ-23), and Innovation Capability Support Program of Shaanxi (No. 2023-CX-TD-62). We thank Instrument Analysis Center of Xi'an Jiaotong University for the assistance with confocal fluorescence imaging.

Author affiliations: [a]Jilin Province Research Center for Engineering and Technology of Spectral Analytical Instruments, College of Chemistry, Jilin University, Changchun 130012, Jilin, People's Republic of China; [b]Institute of Analytical Chemistry and Instrument for Life Science, The Key Laboratory of Biomedical Information Engineering of Ministry of Education, School of Life Science and Technology, Xi'an Jiaotong University, Xi'an 710049, Shaanxi, People's Republic of China; [c]New Cornerstone Science Laboratory, Frontiers Science Center for Transformative Molecules, Zhangjiang Institute for Advanced Study and National Center for Translational Medicine, School of Chemistry and Chemical Engineering, Shanghai Jiao Tong University, Shanghai 200240, People's Republic of China; [d]Institute of Molecular Medicine, Shanghai Key Laboratory for Nucleic Acids Chemistry and Nanomedicine, Renji Hospital, School of Medicine, Shanghai Jiao Tong University, Shanghai 200127, People's Republic of China; and [e]Frontier Institute of Science and Technology, and Interdisciplinary Research Center of Frontier science and technology, Xi'an Jiaotong University, Xi'an 710049, Shaanxi, People's Republic of China

1. T. Yeung *et al.*, Membrane phosphatidylserine regulates surface charge and protein localization. *Science* **319**, 210–213 (2008).
2. T. Otto, P. Sicinski, Cell cycle proteins as promising targets in cancer therapy. *Nat. Rev. Cancer* **17**, 93–115 (2017).
3. S. B. Pollock *et al.*, Highly multiplexed and quantitative cell-surface protein profiling using genetically barcoded antibodies. *Proc. Natl. Acad. Sci. U.S.A.* **115**, 2836–2841 (2018).
4. Y. Ma *et al.*, Spatial imaging of glycoRNA in single cells with ARPLA. *Nat. Biotechnol.* **42**, 608–616 (2024).
5. T. Zhong *et al.*, A Patching and coding lipid raft-localized universal imaging platform. *Chem. Biomed. Imaging* **2**, 135–146 (2024).
6. X. Chen *et al.*, High spatial-resolved heat manipulating membrane heterogeneity alters cellular migration and signaling. *Proc. Natl. Acad. Sci. U.S.A.* **120**, e2312603120 (2023).
7. I.-M. Daumann, P. R. Hiesinger, Lipid rafts, Rab GTPases, and a late endosomal checkpoint for plasma membrane recycling. *Proc. Natl. Acad. Sci. U.S.A.* **120**, e2302320120 (2023).
8. S. Ballweg *et al.*, Regulation of lipid saturation without sensing membrane fluidity. *Nat. Commun.* **11**, 756 (2020).
9. B.-J. Lin *et al.*, Lipid rafts sense and direct electric field-induced migration. *Proc. Natl. Acad. Sci. U.S.A.* **114**, 8568–8573 (2017).
10. S. Alberti, A. A. Hyman, Biomolecular condensates at the nexus of cellular stress, protein aggregation disease and ageing. *Nat. Rev. Mol. Cell Biol.* **22**, 196–213 (2021).
11. N. H. Stillman *et al.*, Protein mimetic 2D FAST rescues alpha synuclein aggregation mediated early and post disease Parkinson's phenotypes. *Nat. Commun.* **15**, 3658 (2024).
12. J. Tyedmers, A. Mogk, B. Bukau, Cellular strategies for controlling protein aggregation. *Nat. Rev. Mol. Cell Biol.* **11**, 777–788 (2010).
13. E. Hallacli *et al.*, The Parkinson's disease protein alpha-synuclein is a modulator of processing bodies and mRNA stability. *Cell* **185**, 2035–2056.e2033 (2022).
14. H. Nan, M. Cai, S. Kuang, Z. Nie, Monitoring of cell membrane microenvironment based on DNA nanodevices. *Chem. Res. Chin. Univ.* **40**, 255–267 (2024).
15. L. Zhao *et al.*, Aptamer-based membrane protein analysis and molecular diagnostics. *Chem. Res. Chin. Univ.* **40**, 173–189 (2024).
16. R. Jalili, J. Horecka, J. R. Swartz, R. W. Davis, H. H. J. Persson, Streamlined circular proximity ligation assay provides high stringency and compatibility with low-affinity antibodies. *Proc. Natl. Acad. Sci. U.S.A.* **115**, E925–E933 (2018).
17. A. Yan *et al.*, Phosphorothioated DNA engineered liposomes as a general platform for stimuli-responsive cell-specific intracellular delivery and genome editing. *Angew. Chem. Int. Ed.* **62**, e202303973 (2023).
18. Y. Su *et al.*, Enhancing cell membrane phase separation for inhibiting cancer metastasis with a stimuli-responsive DNA nanodevice. *Chem. Sci.* **13**, 6303–6308 (2022).
19. Y. Wei *et al.*, Directing the encapsulation of single cells with DNA framework nucleator-based hydrogel growth. *Angew. Chem. Int. Ed.* **63**, e202319907 (2024).
20. S. Liu, S. Li, J. Lin, J. Li, H. Yang, Aptamer-induced-dimerization strategy attenuates AβO toxicity through modulating the trophic activity of PrPC signaling. *J. Am. Chem. Soc.* **144**, 9264–9270 (2022).
21. J. Xue *et al.*, Pairwise proximity-differentiated visualization of single-cell DNA epigenetic marks. *Angew. Chem. Int. Ed.* **60**, 3428–3432 (2020).
22. M. You *et al.*, DNA probes for monitoring dynamic and transient molecular encounters on live cell membranes. *Nat. Nanotechnol.* **12**, 453–459 (2017).
23. H. Liang *et al.*, Nongenetic approach for imaging protein dimerization by aptamer recognition and proximity-induced DNA assembly. *J. Am. Chem. Soc.* **140**, 4186–4190 (2018).
24. X. Chang *et al.*, Construction of a multiple-aptamer-based DNA logic device on live cell membranes via associative toehold activation for accurate cancer cell identification. *J. Am. Chem. Soc.* **141**, 12738–12743 (2019).
25. A. H. Clowsley *et al.*, Detecting nanoscale distribution of protein pairs by proximity-dependent super-resolution microscopy. *J. Am. Chem. Soc.* **142**, 12069–12078 (2020).
26. F. Schueder *et al.*, Super-resolution spatial proximity detection with proximity-PAINT. *Angew. Chem. Int. Ed.* **60**, 716–720 (2021).
27. M. Lundberg, A. Eriksson, B. Tran, E. Assarsson, S. Fredriksson, Homogeneous antibody-based proximity extension assays provide sensitive and specific detection of low-abundant proteins in human blood. *Nucleic Acids Res.* **39**, e102–e102 (2011).
28. S. Fredriksson *et al.*, Protein detection using proximity-dependent DNA ligation assays. *Nat. Biotechnol.* **20**, 473–477 (2002).
29. L. Vistain *et al.*, Quantification of extracellular proteins, protein complexes and mRNAs in single cells by proximity sequencing. *Nat. Methods* **19**, 1578–1589 (2022).
30. X. Yang, L. Yang, D. Yang, M. Li, P. Wang, In situ DNA self-assembly on the cell surface drives unidirectional clustering of membrane proteins for the modulation of cell behaviors. *Nano Lett.* **22**, 3410–3416 (2022).
31. L. Wang *et al.*, Bispecific aptamer induced artificial protein-pairing: A strategy for selective inhibition of receptor function. *J. Am. Chem. Soc.* **141**, 12673–12681 (2019).
32. S. Bi *et al.*, Cancer cell-selective membrane receptor clustering driven by VEGF secretion for in vivo therapy. *J. Am. Chem. Soc.* **145**, 5041–5052 (2023).
33. B. Li, Y. Wang, B. Liu, Transformable DNA nanorobots reversibly regulating cell membrane receptors for modulation of cellular migrations. *ACS Nano* **17**, 22571–22579 (2023).
34. X. Yu *et al.*, ARMOR: Auto-assembled resilient biomimetic calcified ornaments for selective cell protection by dual-aptamer-driven hybridization chain reaction. *Angew. Chem. Int. Ed.* **62**, e202301083 (2023).
35. W. Qin, K. F. Cho, P. E. Cavanagh, A. Y. Ting, Deciphering molecular interactions by proximity labeling. *Nat. Methods* **18**, 133–143 (2021).
36. J. B. Geri *et al.*, Microenvironment mapping via Dexter energy transfer on immune cells. *Science* **367**, 1091–1097 (2020).
37. J. V. Oakley *et al.*, Radius measurement via super-resolution microscopy enables the development of a variable radii proximity labeling platform. *Proc. Natl. Acad. Sci. U.S.A.* **119**, e2203027119 (2022).
38. K. F. Cho *et al.*, Split-TurboID enables contact-dependent proximity labeling in cells. *Proc. Natl. Acad. Sci. U.S.A.* **117**, 12143–12154 (2020).
39. D. Wu *et al.*, Profiling surface proteins on individual exosomes using a proximity barcoding assay. *Nat. Commun.* **10**, 3854 (2019).
40. F. Karlsson *et al.*, Molecular pixelation: Spatial proteomics of single cells by sequencing. *Nat. Methods* **21**, 1044–1052 (2024).
41. F. Chen *et al.*, Cellular macromolecules-tethered DNA walking indexing to explore nanoenvironments of chromatin modifications. *Nat. Commun.* **12**, 1965 (2021).
42. E. Ambrosetti *et al.*, A DNA-nanoassembly-based approach to map membrane protein nanoenvironments. *Nat. Nanotechnol.* **16**, 85–95 (2021).
43. S. Woo, S. K. Saka, F. Xuan, P. Yin, Molecular robotic agents that survey molecular landscapes for information retrieval. *Nat. Commun.* **15**, 3293 (2024).
44. Y. Liu *et al.*, Bidirectional linkage of DNA barcodes for the multiplexed mapping of higher-order protein interactions in cells. *Nat. Biomed. Eng.* **8**, 909–923 (2024).
45. M. Dai, R. Jungmann, P. Yin, Optical imaging of individual biomolecules in densely packed clusters. *Nat. Nanotechnol.* **11**, 798–807 (2016).
46. L. DeFazio-Eli *et al.*, Quantitative assays for the measurement of HER1-HER2 heterodimerization and phosphorylation in cell lines and breast tumors: Applications for diagnostics and targeted drug mechanism of action. *Breast Cancer Res.* **13**, R44 (2011).
47. S. G. Elias *et al.*, Imaging features of HER2 overexpression in breast cancer: A systematic review and meta-analysis. *Cancer Epidemiol. Biomar. Preven.* **23**, 1464–1483 (2014).
48. A. Harada *et al.*, A chromatin integration labelling method enables epigenomic profiling with lower input. *Nat. Cell Biol.* **21**, 287–296 (2019).
49. M. Levitt, How many base-pairs per turn does DNA have in solution and in chromatin? Some theoretical calculations *Proc. Natl. Acad. Sci. U.S.A.* **75**, 640–644 (1978).
50. B. Tinland, A. Pluen, J. Sturm, G. Weill, Persistence length of single-stranded DNA. *Macromolecules* **30**, 5763–5765 (1997).
51. A. He *et al.*, Structure-based investigation of a DNA aptamer targeting PTK7 reveals an intricate 3D fold guiding functional optimization. *Proc. Natl. Acad. Sci. U.S.A.* **121**, e2404060121 (2024).
52. D. P. Buser, K. D. Schleicher, C. Prescianotto-Baschong, M. Spiess, A versatile nanobody-based toolkit to analyze retrograde transport from the cell surface. *Proc. Natl. Acad. Sci. U.S.A.* **115**, E6227–E6236 (2018).
53. T. Bing *et al.*, Aptameric probe specifically binding protein heterodimer rather than monomers. *Adv. Sci.* **6**, 1900143 (2019).
54. J. Li *et al.*, Amplified visualization of protein-specific glycosylation in zebrafish via proximity-induced hybridization chain reaction. *J. Am. Chem. Soc.* **140**, 16589–16595 (2018).
55. L. Zhu *et al.*, Coupling aptamer-based protein tagging with metabolic glycan labeling for in situ visualization and biological function study of exosomal protein-specific glycosylation. *Angew. Chem. Int. Ed.* **60**, 18111–18115 (2021).
56. X. Zhao *et al.*, Data from "Proximity-Activated DNA scanning encoded sequencing for massive access to membrane proteins nanoscale organization." NCBI SRA. https://www.ncbi.nlm.nih.gov/sra/?term=PRJNA1185922. Deposited 14 November 2024.
57. X. Zhao *et al.*, Data from "Proximity-Activated DNA scanning encoded sequencing for massive access to membrane proteins nanoscale organization." NCBI SRA. https://www.ncbi.nlm.nih.gov/sra/?term=PRJNA1221128. Deposited 8 February 2025.